Bimetallic Conjugated Microporous Polymer Derived B, N-doped Porous Carbon Wrapped Co_3Fe_7 alloy Composite as Bifunctional Oxygen Electrocatalyst for Breathing Zn-air battery

Jinli Dou,[a]† Haotian Luo,[a]† Chunli Zhang,[b]† Jingjing Lu,† [a] Xiujuan Luan,[a] Wenxue Guo,[a] Teng Zhang,[a] Jingkun Bai,*[d] Weiwei Bian*[a], Xueli Zhang,*[c] Baolong Zhou*[a]

[a]*School of Pharmacy, Weifang Medical University, Weifang, 261053, Shandong, P. R. China.*

[b]*Western Pharmacy, Anqiu Hospital of Traditional Chinese Medicine, Weifang, Shandong, P. R. China.*

[c]*Department of Histology and Embryoiogy, Weifang Medical University, 261053, Shandong, China.*

[d]*School of Bioscience and Technology, Weifang Medical University, Weifang, 261053, PR China*

E-mail: zhoubaolong@wfmc.edu.cn

†These authors make equal contribution to this article.

Contents

Section 1. Materials and Characterization

Materials

Chemicals were purchased were purchased from commercial suppliers and were used without further purification unless otherwise noted. *N,N*-Dimethylformamide (DMF) anhydrous solvent was distilled from commercial DMF withCaH2. Pyrrole was distilled before use.

Characterization

^{1}H and ^{13}C NMR spectra of prepared monomers were recorded on an Avance Bruker DPX 400 (400 MHz) in the solvent of $CDCl_3$. Solid-state ^{13}C CP/MAS NMR were collected on Bruker SB Avance III 500 MHz spectrometer. Fourier Transform Infrared Spectroscopy (FTIR) was performed on KBr pellets in the range from 4000 to 400 cm^{-1} using Spectrum Spotlingt 400. The elemental analysis was performed by Elementar Vario EL III (Elementar Analysensysteme GmbH, Germany) based on JY/T 017-1996 general rules for elemental analyzer. Thermo-gravimetric analysis (TGA) were recorded using NETZSCH STA 449C analyzer from 25 ^{o}C to 900 ^{o}C at a heating rate of 10 ^{o}C min^{-1} under the protection of N_2. The morphologies of powder samples were evaluated by field-emission scanning electron Microscopy (FESEM, Ultra 55) and transmission electron microscopy (TEM, Tecnai G2 20 TWIN) via dipping the prepared samples on a Cu-net. The adsorption and desorption measurements for N_2 were performed on a Belsorp max analyzer (Japan) at low temperature of -273K. Before test, all these samples were degassed overnight under high vacuum at the temperature of 150 ^{o}C to remove the solvent or the water absorbed in the porous skeleton. X-ray Photoelectron Spectroscopy (XPS) was conducted on XPSESCALAB 250Xi analyser.

X-ray diffraction (XRD) parameters were obtained using a Rigaku-DMAX 2500 diffractometer at a rate of 5° min^{-1} from 5° to 80°.

Section 2. Experimental Details

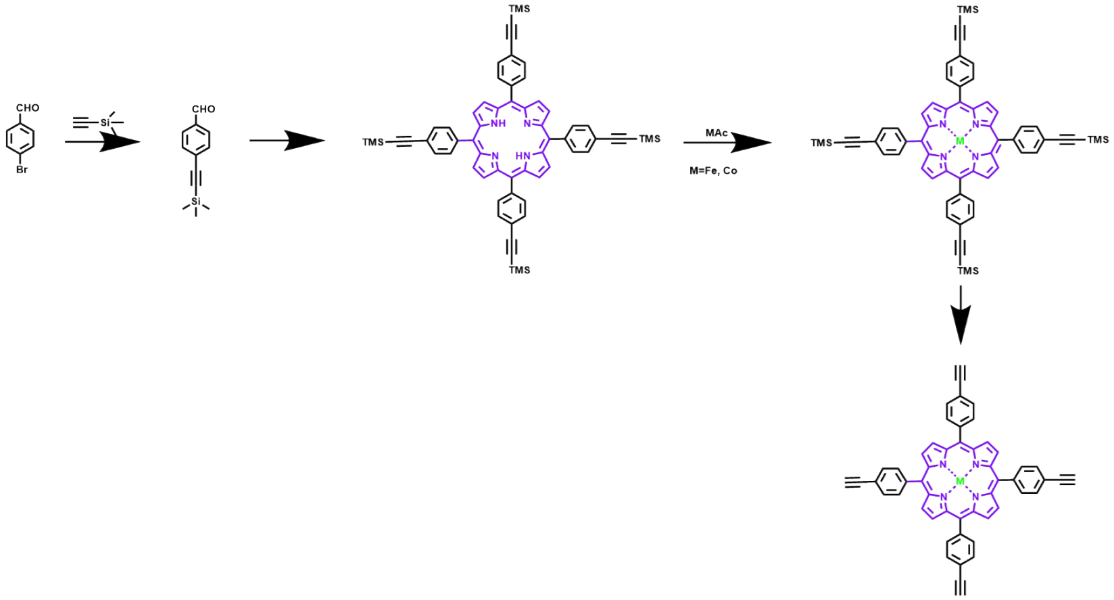

Scheme S1. Synthetic routes of TEPP-M.

Synthesis of 4-(Trimethylsilyl)ethynyl]benzaldehyde

A solution of 4-bromobenzaldehyde (18.5 g, 100 mmol), $PdCl_2(PPh_3)_2$ (510 mg, 0.727 mmol), and CuI (0.228 mg, 1.20 mmol) in a mixture of 100 mL of dry THF and 28 mL of triethylamine was prepared in a 250 mL round-bottom flask degassed and stirred under N_2 for 5 min at room temperature. Trimethylsilylacetylene (14.7 g, 150 mmol) was added, the reaction was stirred at 65 °C overnight. The crude mixture was dissolved in 100 mL dichloromethane and washed with 1 × 100 mL H_2O, 1 × 100 mL of 10% HCl solution, 1 × 100 mL of H_2O. The organic phase was dried over Na_2SO_4 and filtered, and the solvent was removed. The crude mixture was purified by column chromatography (hexanes/dichloromethane 2:1) providing a colorless solid. (19.0 g, 95%).

Synthesis of 5,10,15,20-Tetrakis(4-[(trimethylsilyl)ethynyl]-phenyl)porphyrin.

A solution of 4-[(trimethylsilyl)ethynyl]-benzaldehyde (17.5 g, 86.5 mmol) in propionic acid (ca. 360 mL) was brought to reflux temperature. Then, Pyrrole (6 mL, 86.4 mmol) was added. The mixture was stirred at reflux for 3 h, after which it was allowed to cool to room temperature. A black solid precipitated and the suspension was allowed to stand overnight. The black liquid was removed by filtration and the remaining black solid was washed with methanol until the filtrate was colorless (Yield: 5.9 g, 27.3%).

^{1}H NMR ($CDCl_3$, ppm): -2.84 (NH, s, 2H), 0.372 (Si-CH_3, s, 36H), 7.86 (m-ArH, d, 3J = 7.80 Hz, 8H); 8.14 (o-ArH, d, 3J = 7.80 Hz, 8H); 8.81 (b-H, s, 8H).

Synthesis of 5,10,15,20-Tetrakis(4-(ethynylphenyl)-porphyrin.

5,10,15,20-Tetrakis(4-(trimethylsilyl)ethynyl-phenyl)porphyrin (3 g, 3 mmol) was dissolved in 200 mL of THF. Then, 15 mL of TBAF was dropped in the solution at -78 °C. The temperature was raised from -78 °C to room temperature slowly and kept overnight. 200 mL H_2O was added and extract with 3 × 200 mL of $CHCl_3$. The organic phase was collected and dried with anhydrous Na_2SO_4 and evaporated to dry to get the product as light yellow solid (Yield: 2.1 g, 98.5%). ^{1}H-NMR (CDCl3, ppm): -2.83 (NH, s, 2H), 3.33 (CCH, s, 4H),7.90 (m-ArH, d, 3J = 8.40 Hz, 8H); 8.17 (o-ArH, d, 3J = 8.40 Hz, 8H); 8.84 (b-H, s, 8H).

Synthesis of 5,10,15,20-Tetrakis(4-(ethynylphenyl)-porphyrin-cobalt.

5,10,15,20-Tetrakis(4-(ethynyl-phenyl)-porphyrin (0.937 g,1.32 mmol) was dissolved in70 mL of DMF. $Co(OAc)_2{\cdot}4H_2O$ (0.328 g, 1.32 mmol) was added into the reaction system. The solution was heated to reflux for 1 h and then cooled to room temperature. Then, 100 mL MeOH was added and a purple precipitate was collected. After recrystallizing with $CHCl_3$ and MeOH, a purple solid product was collected (Yield: 24%).

Synthesis of 5,10,15,20-Tetrakis(4-(ethynylphenyl)-porphyrin-iron.

The route for the synthesis of 5,10,15,20-Tetrakis(4-(ethynylphenyl)-porphyrin]iron was as the same as the procedure of [5,10,15,20-tetrakis(4-(ethynylphenyl)porphyrin]cobalt. 5,10,15,20-Tetrakis(4-(ethynyl-phenyl)porphyrin (0.937 g,1.32 mmol) was dissolved in 70 mL of DMF and $Fe(OAc)_2$(0.229 g, 1.32 mmol) was added. Yield:20.7%.

Synthesis of sample 2

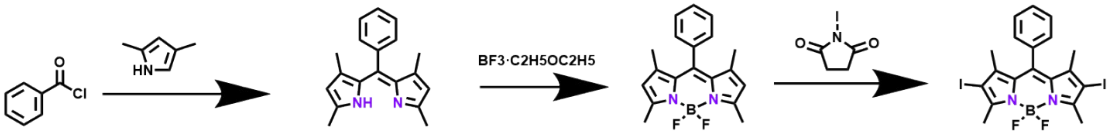

Scheme S2. Synthetic routes of Boidpy-2I.

2,6-Diiodo-1,3,5,7-tetramethyl-8-phenyl-4,4-difluoroboradiazaindacene

Under an argon atmosphere, benzoyl chloride (2.8 g, 0.021 mol) and 2,4-dimethylpyrrole (4 mL, 3.7 g, 0.04 mol) were added to dry dichloromethane (150 mL) using a syringe. The mixture was stirred at room temperature overnight, then Et_3N (20 mL) and $BF_3{\cdot}Et_2O$ (20 mL) were added under ice-cold conditions, and the reaction mixture was stirred for 1 h. Then, the mixture was poured into water (200 mL), and the organic layer was collected, dried over anhydrous Na_2SO_4, and evaporated under reduced pressure. The crude product was purified by column chromatography on silica gel (dichloromethane/n-hexane=1:1, v/v) to give compound 1,3,5,7-tetramethyl-8-phenyl-4,4-difluoroboradiazaindacene as a red powder (yield: ~20%). To a solution of compound 1,3,5,7-tetramethyl-8-phenyl-4,4-difluoroboradiazaindacene (200 mg, 0.62 mmol) in dry dichloromethane (25 mL) was added excess N-iodosuccinimide (NIS; 558 mg, 2.48 mmol). The mixture was stirred at room temperature for about 30 min (monitored by TLC until the starting material had been

completely consumed). The reaction mixture was then concentrated under vacuum, and the crude product was purified by column chromatography on silica gel (n-hexane/dichloromethane=2:1, v/v). The red band was collected and the solvent was removed under reduced pressure to obtain a red solid (yield: ~70%).

Synthesis of BP-CMP

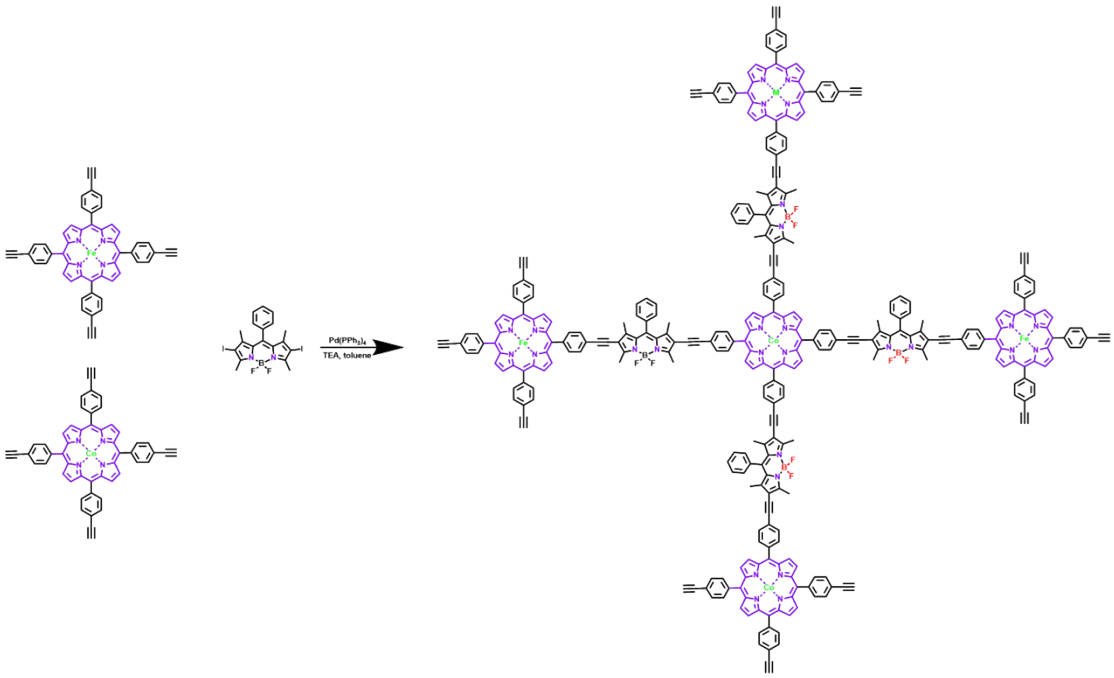

TEPP-Fe (64.0 mg, 0.085 mmol), TEPP-Co (65.0 mg, 0.085 mmol) and BODIPY-2I (230 mg, 0.34 mmol) were dissolved in anhydrous solvent (DMF: TEA=1:1, 8.0 mL). After the mixture was degassed by three freeze-pump-thaw cycles to exclude the oxygen, $Pd(PPh_3)_4$ (25 mg, 0.016 mmol) and CuI (7.0 mg, 0.04 mmol) were added to the system under N_2 protection. The reaction took place in a degassed Pyrex tube (10 mL) through at least three freeze-pump-thaw cycles and followed by sealing off and heating at 150 °C for 72 h. Once the reaction is complete, the precipitate was thoroughly washed with THF, chloroform, and acetone.

Synthesis of P-CMP

As a similar procedure of the preparation of BP-CMP, P-CMP was obtained by TEPP-Fe (64 mg,

0.085 mmol), TEPP-Co (65 mg, 0.085 mmol) and 1,4-dibromobenzene (0.708 g, 3.0 mmol) with a yield of 70%.

Electrochemical Measurements

All electrochemical tests were performed at room temperature using standard three-chamber cells to record the electrode pairs of platinum grid, and the Ag/AgCl electrode saturated with KCl or saturated calomel electrode (SCE) was applied as the reference electrode. All the potentials were referenced to the reversible hydrogen electrode (RHE) scale according to the Nernst equation:

$$E_{(RHE)} = E_{(Ag/AgCl)} + 0.059 \times pH + 0.197 \text{ V, at } 25°C$$

$$E_{(RHE)} = E_{(Hg/HgOl)} + 0.059 \times pH + 0.098 \text{ V, at } 25°C.$$

The working electrode can be either a rotating disk electrode (RDE) composed of a glass carbon disk (diameter 5.0mm) or a rotating ring disk electrode (RRDE) composed of a glass carbon disk (diameter 3 mm) surrounding an outer platinum ring (inner diameter 5 mm, outer diameter 7 mm). The catalyst ink is loaded on the working electrode surface. The catalyst inks and commercially available Pt/C (20 wt%) inks are made by dispersing 5.0 mg of the fresh-prepared catalyst or commercially available Pt/C (20 wt%) in an ultrasonic bath to a 500 μL solvent mixture (25 μL Naffion solution (5 wt%), 75 μL H_2O, and 400 μL ethanol) to a uniform suspension. Then suck the catalyst ink (8 μL) through a straw onto the glass carbon surface of RDE or RRDE and let it dry in the air at room temperature.

The catalytic activity of the catalyst was measured by cyclic voltammetry (CV) and rotary disk electrode (RDE) at CHI-760 electrochemical station. All tests were carried out under alkaline (0.1 M KOH), neutral (0.1 M PBS), or acidic conditions (0.1 m $HClO_4$). CV was

measured at 50 mV s^{-1} in various electrolytes saturated with O_2 or Ar. The RDE/RRDE tests were examined with a scanning rate of 5 mV s^{-1} at different speeds ranging from 400 to 2500 rpm. The K-L equation was applied to investigate the ORR kinetic parameters. The K-L equation can be described as follows:

$$\frac{1}{J} = \frac{1}{J_L} + \frac{1}{J_K} = \frac{1}{B\,\omega^{1/2}} + \frac{1}{J_K} \qquad (1)$$

Where J is the current density，J_L is the current that was measured; J_K represents the kinetic-limiting current and ω is the rotation speeds of electrode.

$$B = 0.62nFC_0(D_0)^{2/3}V^{-1/6} \qquad (2)$$

In equation 2, n is the total number of transferred electrons during the oxygen reduction process; F is Faradaic constant (F = 96485 C mol^{-1}), C_0 is the O_2 concentration (solubility) in 0.1 M KOH electrolyte (1.2 × 10^{-6} mol cm^{-3}); D_0 is the O_2 diffusion coefficient (1.90 × 10^{-5} cm^2 s^{-1}), and V is the kinematic viscosity of the O_2 saturated 0.1 M KOH solution (0.01 cm^2 s^{-1}). For the RRDE measurements, the disk electrode was also scanned with a rate of 5 mV s^{-1} at a constant ring potential of 1.5 V *vs.* RHE. The peroxide percentage (H_2O_2 yields) and the transferred number of electron (n) were calculated according to the following equations (3) - (4):[S3]

$$H_2O_2\% = 200\frac{Ir/N}{Id + Ir/N} \qquad (3)$$

$$N = 4\frac{Id}{Id + Ir/N} \qquad (4)$$

In eqution 3 and 4, I_d is the disk current, and I_r refers to the ring current and N represents the current collection efficiency of the Pt ring (N=0.4581).

Fabrication of Zn-Air Battery

Typically, Zinc-Air battery was assembled by employing zinc plate as anode, electrocatalyst containing gas diffusion layer as air electrode, aqueous solution containing 6 M KOH and 0.2M $Zn(OAc)_2$ as electrolyte. For the fabrication of air electrode, the isopropanol ink containing electrocatalysts, ethanol and nafion was homogenously sprayed onto a carbon paper with a catalyst loading of 1 mg cm^{-2}. For comparison, the commercial Pt/C or the mixture of commercial Pt/C-IrO_2 (in a mass ratio of 1:1) was also employed to fabricate ZABs as benchmarks.

Section 3. Liquid NMR

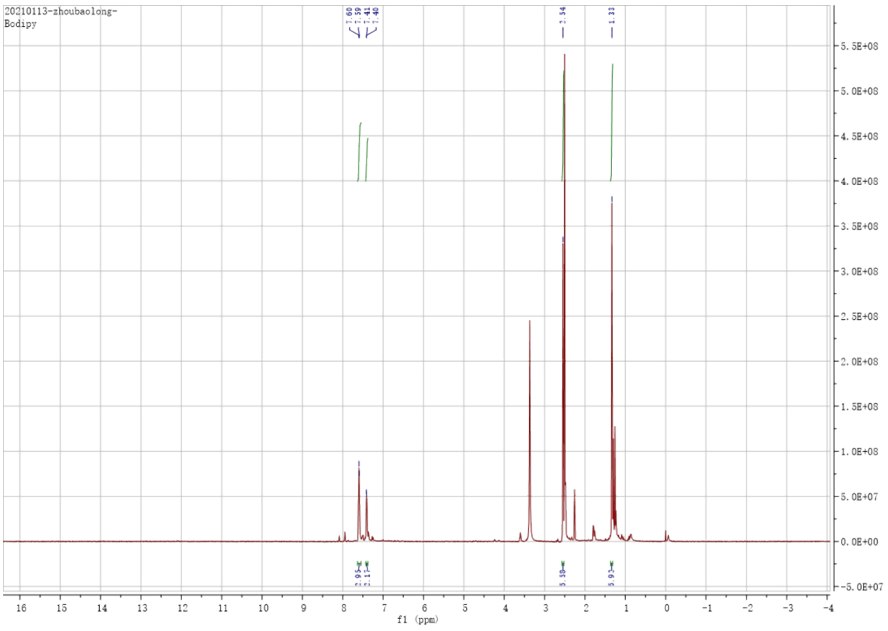

Figure S1. ^{1}H- NMR spectrum of Bodipy-2I

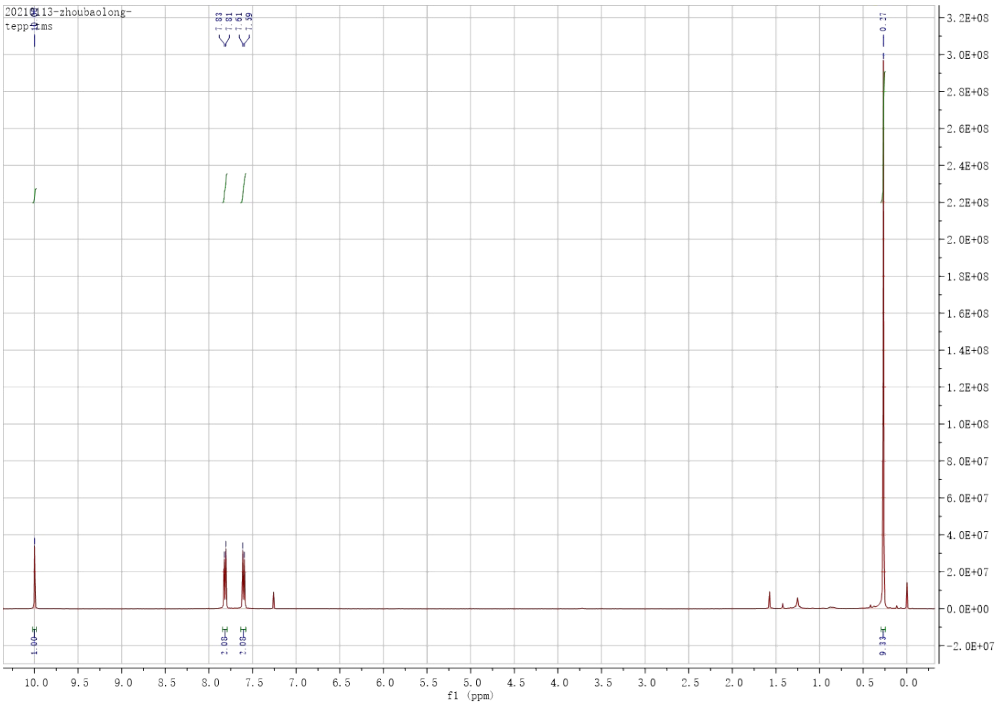

Figure S2. ^{1}H- NMR spectrum of [4-(Trimethylsilyl)ethynyl]benzaldehyde.

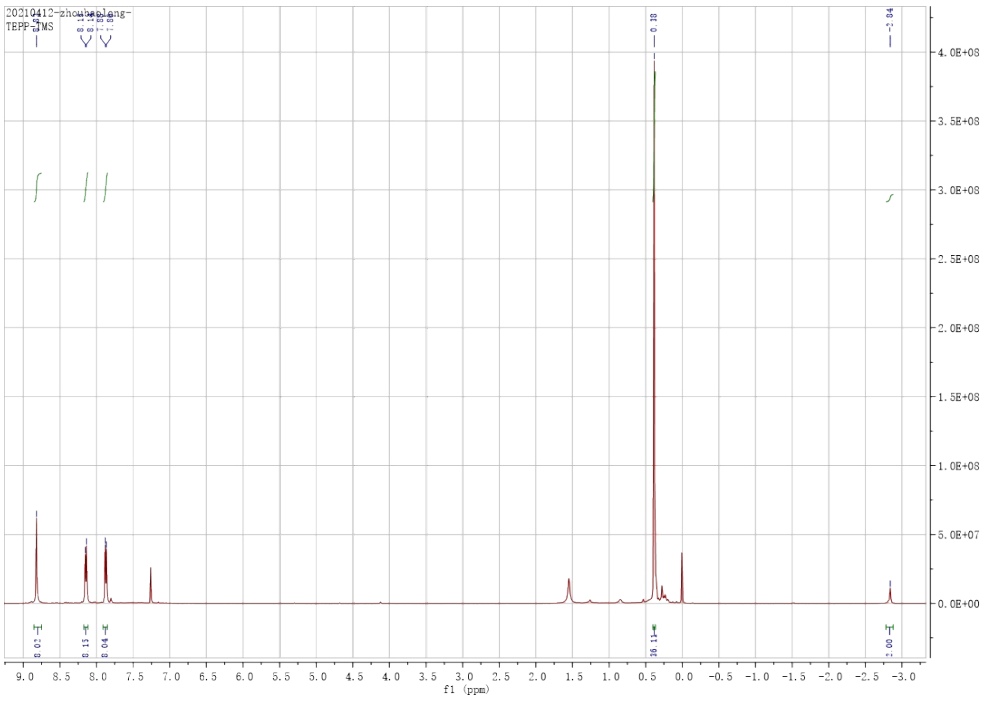

Figure S3. ^{1}H-NMR spectrum of 5,10,15,20-Tetrakis(4-[(trimethylsilyl)ethynyl]-phenyl)porphyrin

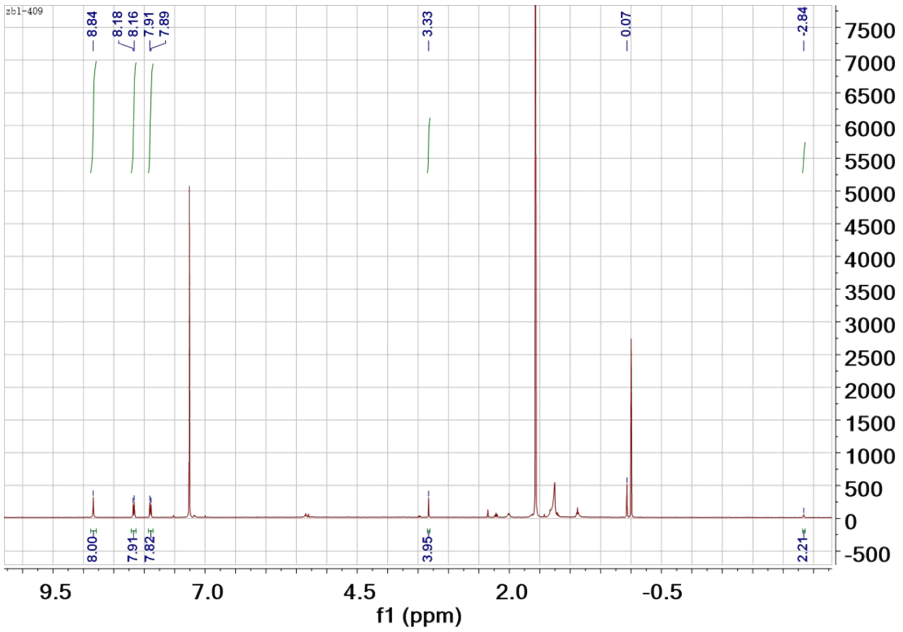

Figure S4. ^{1}H-NMR spectrum of 5,10,15,20-Tetrakis(4-(ethynylphenyl)-porphyrin

Section 4. TG and TEM

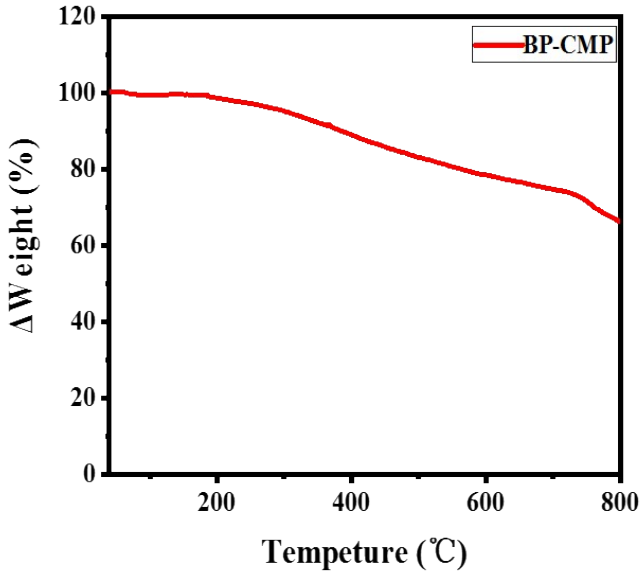

Figure S5. TG curves of BP-CMP.

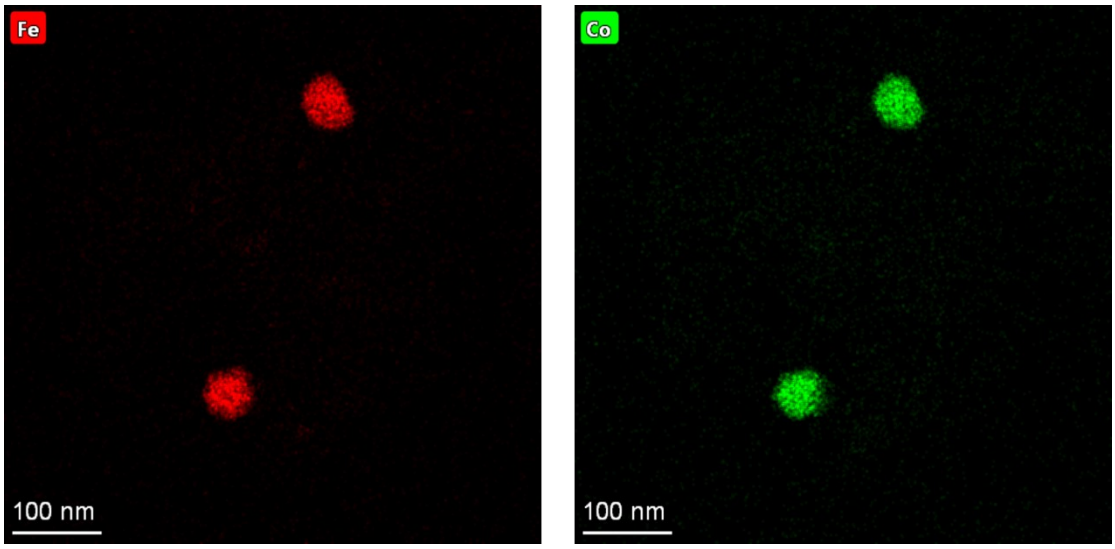

Figure S6. Elemental mapping images BP-800 at a scale bar of 100 nm.

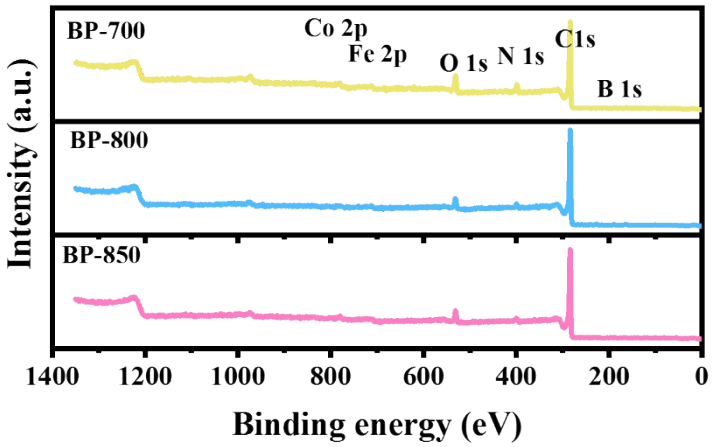

Figure S7. XPS survey of BP-700, BP-800 and BP-850 catalysts.

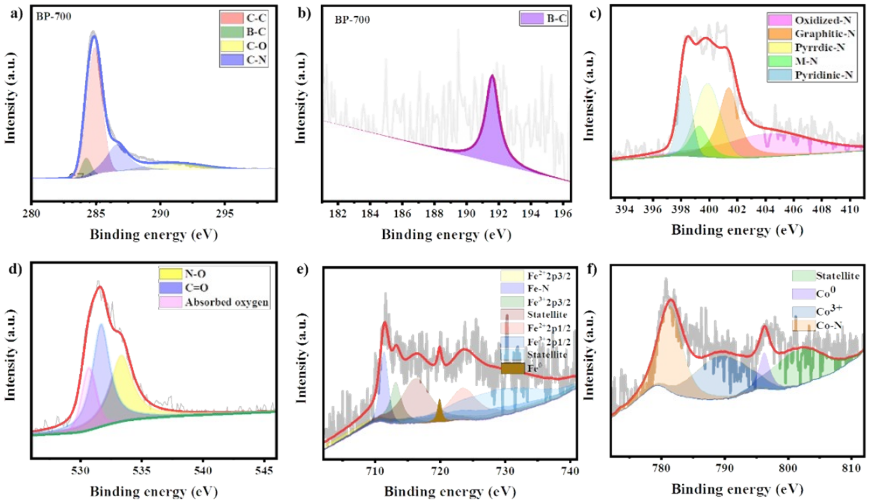

Figure S8. XPS of BP-700. a) High-resolution XPS of C 1s spectra for BP-700; b) High-resolution XPS of B 1s for BP-700; c) High-resolution XPS spectra of N 1s spectra for BP-700; d) High-resolution XPS spectra of O 1s spectra for BP-700; e) High-resolution XPS spectra of Fe 2p spectra for BP-700; f) High-resolution XPS spectra of Co 2p spectra for BP-700.

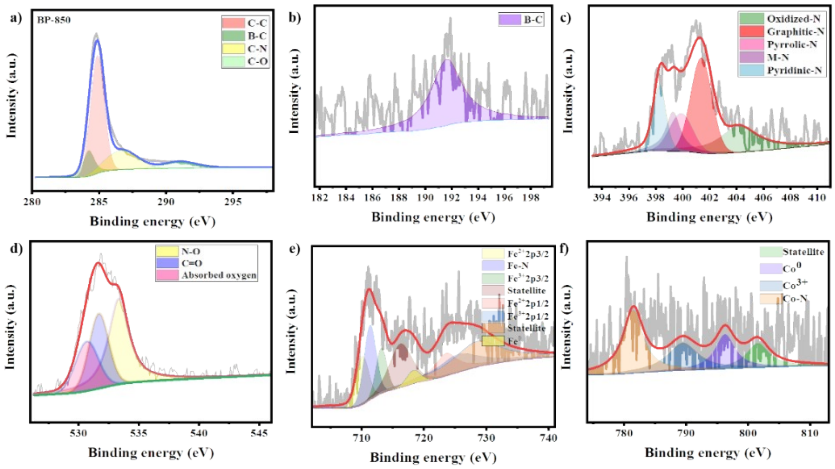

Figure S9. XPS of BP-850. a) High-resolution XPS of C 1s spectra for BP-850; b) High-resolution XPS of C 1s for BP-850; c) High-resolution XPS spectra of N 1s spectra for BP-850; d) High-resolution XPS spectra of O1s spectra for BP-850; e) High-resolution XPS spectra of Fe 2p spectra for BP-850; f) High-resolution XPS spectra of Co 2p spectra for BP-850.

Section 7. Electrochemical Performance

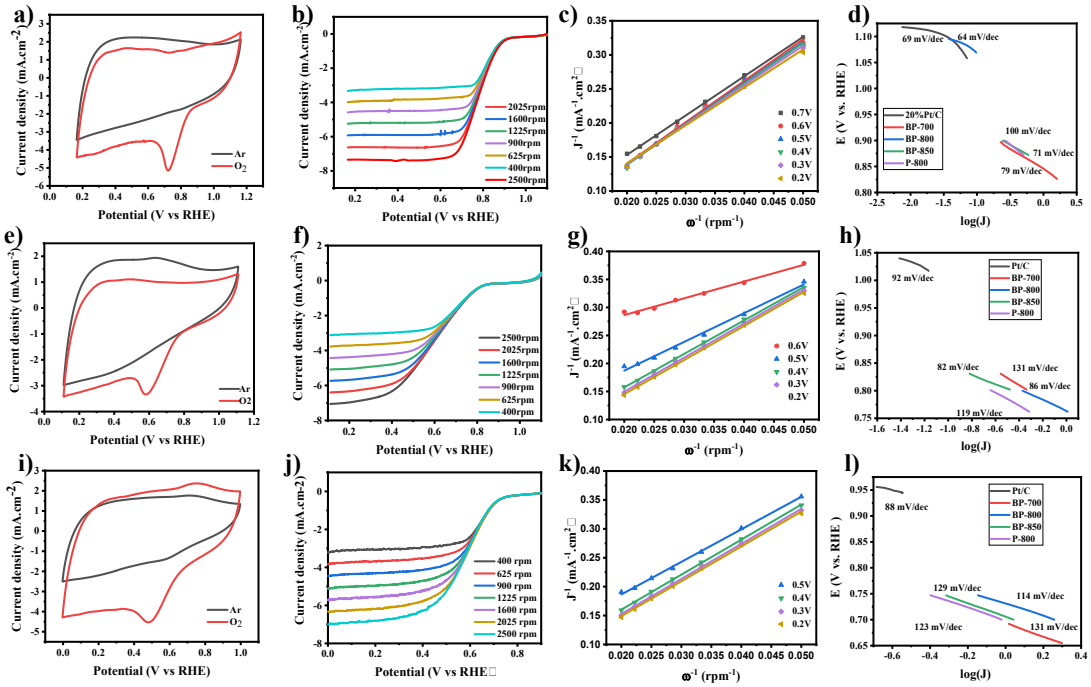

Figure S10. Electrochemical performance of BP-800 in various electrolytes form alkaline conditions to acidic conditions. a) Cyclic voltammograms (CV) of BP-800 obtained in O_2 and Ar saturated in 0.1 M KOH; b) LSV curves of BP-700 at different rotation rates in 0.1 M KOH ; c) K-L plot and the corresponding electron transfer numbers for BP-700 in 0.1 M KOH; d) The Tafel slopes of ORR on BP-700, BP-800, BP-850,P-800 and Pt/C in a) 0.1 M KOH; e) Cyclic voltammograms (CV) of BP-700 obtained in O_2 and Ar saturated in 0.1 M PBS; f) LSV curves of BP-700 at different rotation rates in 0.1 M PBS, g) K-L plot and the corresponding electron transfer numbers for BP-700 in 0.1 M PBS; h) The Tafel slopes of ORR on BP-700, BP-800, BP-850,P-800 and Pt/C in a) 0.1 M PBS i) Cyclic voltammograms (CV) obtained in O_2 and Ar saturated in 0.1 M $HClO_4$; j) LSV curves of BP-700 at different rotation rates in 0.1 M $HClO_4$, k) K-L plot and the corresponding electron transfer numbers for BP-700 in 0.1 M $HClO_4$; l) The Tafel slopes of ORR on BP-700, BP-800, BP-850,P-800 and Pt/C in a) 0.1 M $HClO_4$

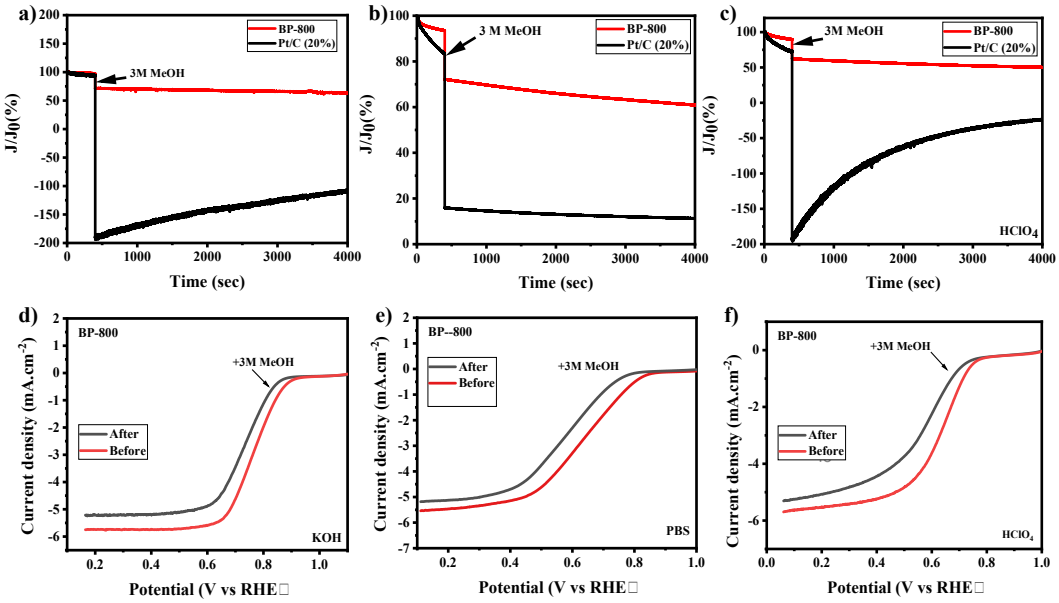

Figure S11. Comparison of methanol immunity of BP-800 and commercial Pt/C. a) Comparison of methanol tolerance test between BP-800 and Pt/C (20%) in a)0.1M KOH, b) 0.1M PBS and c) 0.1M $HClO_4$ saturated O_2 ;b) LSV curve of BP-800 measured before and after the injection of 3 M methanol in a)0.1M KOH, b) 0.1M PBS and c) 0.1M $HClO_4$ saturated O_2.

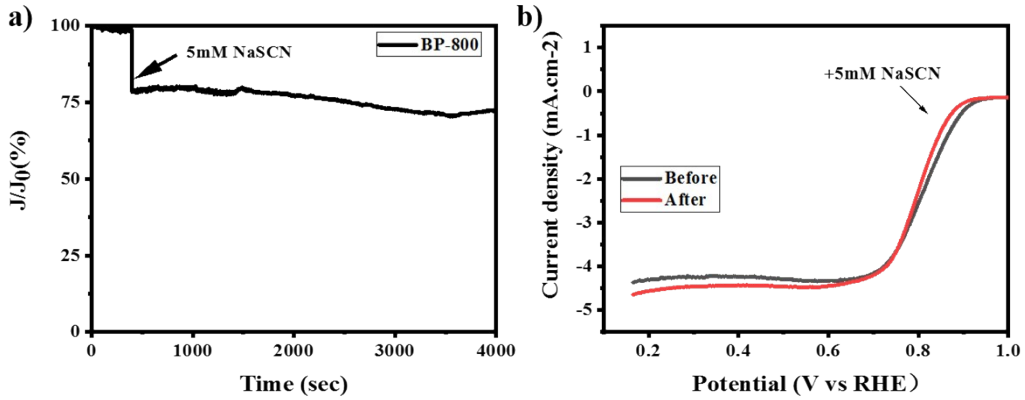

Figure S12. a) Current-time (i-t) curves and (b) RDE results of BP-800 in O_2-saturated 0.1 M KOH solution (without and with SCN^-)

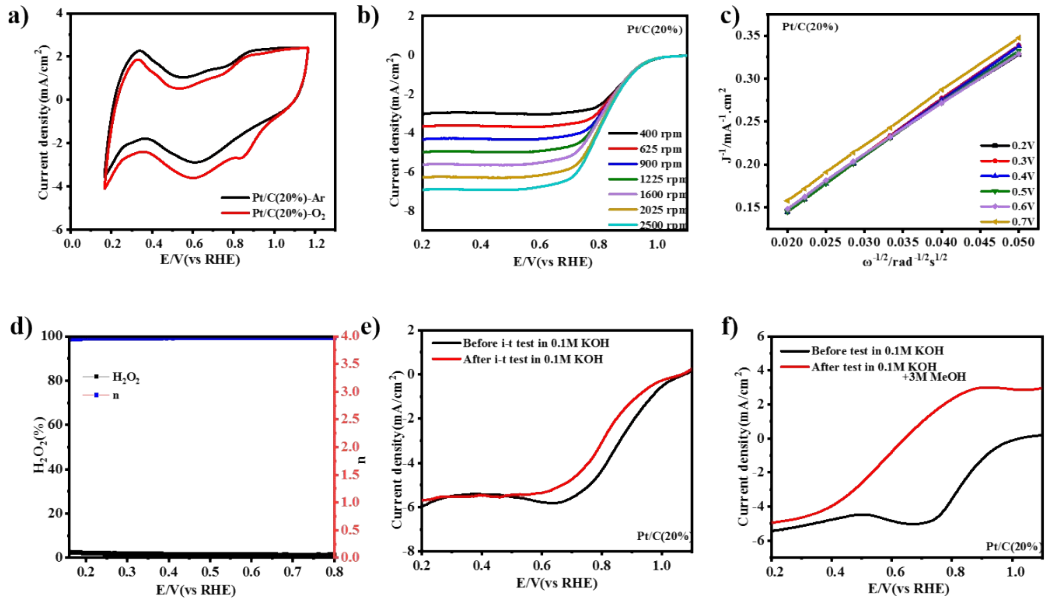

Figure S13. a) CV curves of commercial Pt/C (20%) on a glassy carbon electrodes in 0.1 M KOH saturated with O_2 or Ar at a sweep rate of 50 mV s^{-1}; b) LSV of commercial Pt/C (20%) at various rotation speeds; c) K-L plots curves of commercial Pt/C (20%); d) Percentage of hydrogen peroxide yield and the electron transfer number (n) of Pt/C at different potentials; e) Polarization curves of Pt/C (20%) measured by RDE in O_2-saturated 0.1 M KOH before (black line) and after (red line) the i-t (20000 s) experiments; f) LSV curve of Pt/C measured before and after the injection of 3 M methanol.

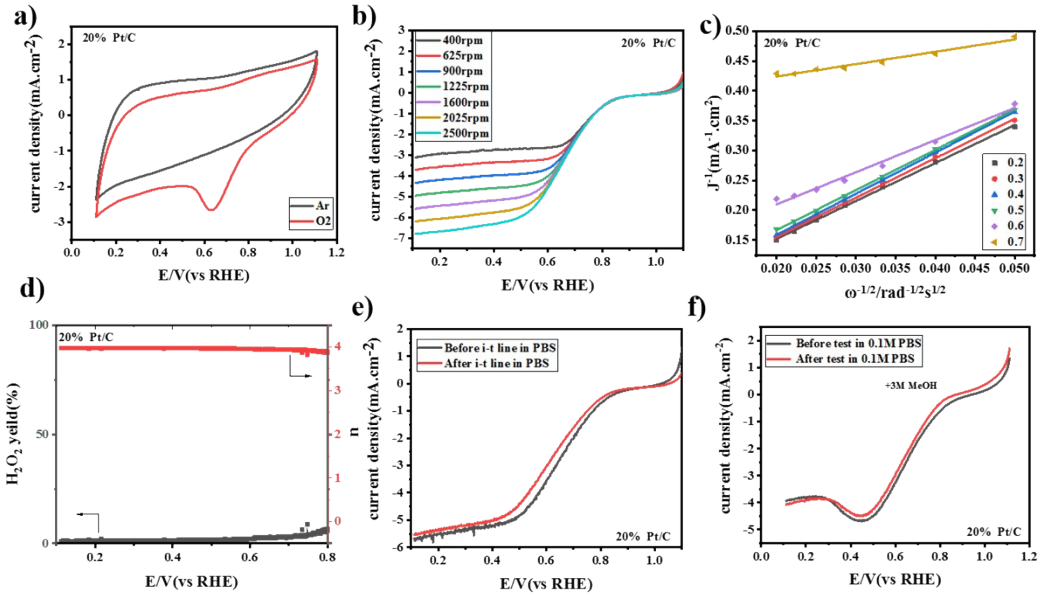

Figure S14. Electrochemical performance of commercial Pt/C in neutral conditions. a) CV curves of commercial Pt/C (20%) on glassy carbon electrodes in water solution of 0.1 M PBS saturated with O_2 or argon at a sweep rate of 50 mV s^{-1}. b) LSV of commercial Pt/C (20%) at different rotation speeds; c) K-L plots curves of Pt/C (20%) at different potentials; d) Percentage of hydrogen peroxide yield and the electron transfer number (n) of Pt/C (20%) at different potentials; e) Polarization curves of Pt/C (20%) measured by RDE in O_2-saturated 0.1 M PBS before (black line) and after (red line) the i-t (20000 s) experiments; f) LSV curve of Pt/C (20%) measured before and after the injection of 3 M methanol.

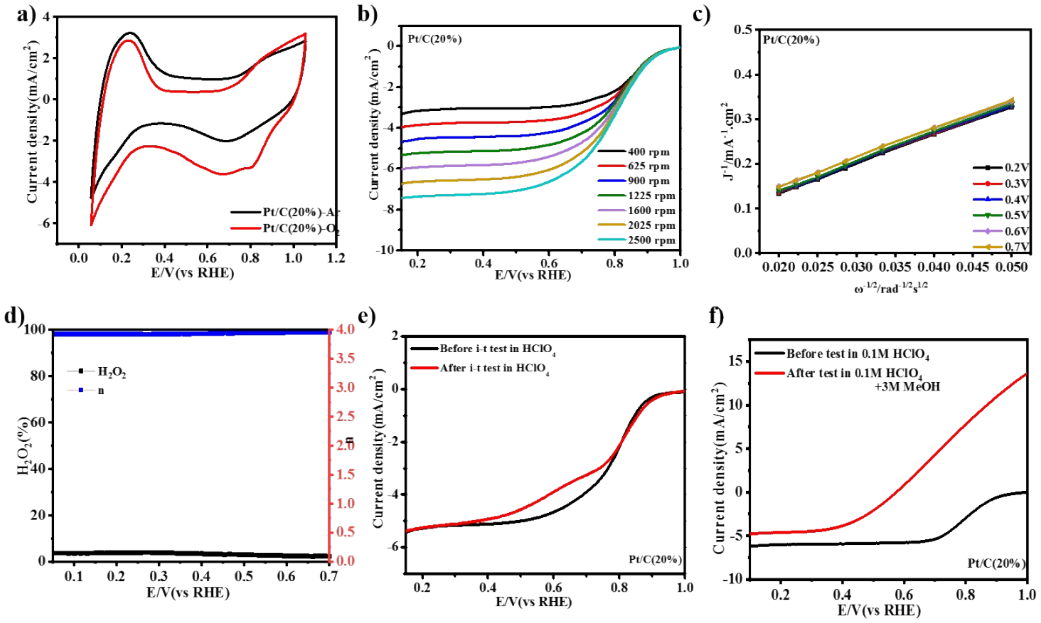

Figure S15. Electrochemical performance of commercial Pt/C in acidic conditions. a) CV curves of commercial Pt/C (20%) on glassy carbon electrodes in water solution of 0.1 M $HClO_4$ saturated with O_2 or argon at a sweep rate of 50 mV s^{-1}. b) LSV of commercial Pt/C (20%) at different rotation speeds; c) K-L plots curves of Pt/C (20%) at different potentials; d) Percentage of hydrogen peroxide yield and the electron transfer number (n) of Pt/C (20%) at different potentials; e) Polarization curves of Pt/C (20%) measured by RDE in O_2-saturated 0.1 M $HClO_4$ before (before line) and after (red line) the i-t (20000 s) experiments; f) LSV curve of Pt/C (20%) measured before and after the injection of 3 M methanol.

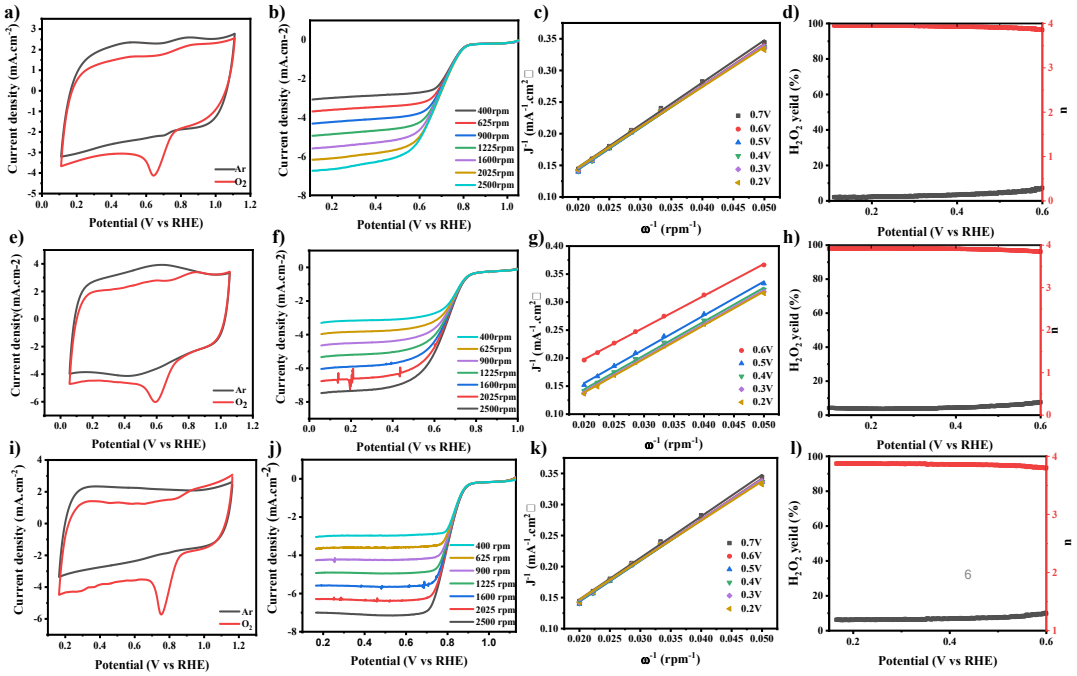

Figure S16. Electrochemical performance of BP-700 in various electrolytes form alkaline conditions to acidic conditions. a) Cyclic voltammograms (CV) of BP-700 obtained in O_2 and Ar saturated in 0.1 M KOH; b) LSV curves of BP-700 at different rotation rates in 0.1 M KOH ; c) K-L plot and the corresponding electron transfer numbers for BP-700 in 0.1 M KOH; d) Percentage of hydrogen peroxide yield and the electron transfer number (n) of BP-700 at different potentials in 0.1 M KOH; e) Cyclic voltammograms (CV) of BP-700 obtained in O_2 and Ar saturated in 0.1 M PBS; f) LSV curves of BP-700 at different rotation rates in 0.1 M PBS; g) K-L plot and the corresponding electron transfer numbers for BP-700 in 0.1 M PBS; h) Percentage of hydrogen peroxide yield and the electron transfer number (n) of BP-700 at different potentials in 0.1 M PBS; i) Cyclic voltammograms (CV) obtained in O_2 and Ar saturated in 0.1 M $HClO_4$; j) LSV curves of BP-700 at different rotation rates in 0.1 M $HClO_4$; k) K-L plot and the corresponding electron transfer numbers for BP-700 in 0.1 M $HClO_4$; l) Percentage of hydrogen peroxide yield and the electron transfer number (n) of BP-700 at different potentials in 0.1 M $HClO_4$ electrolytes.

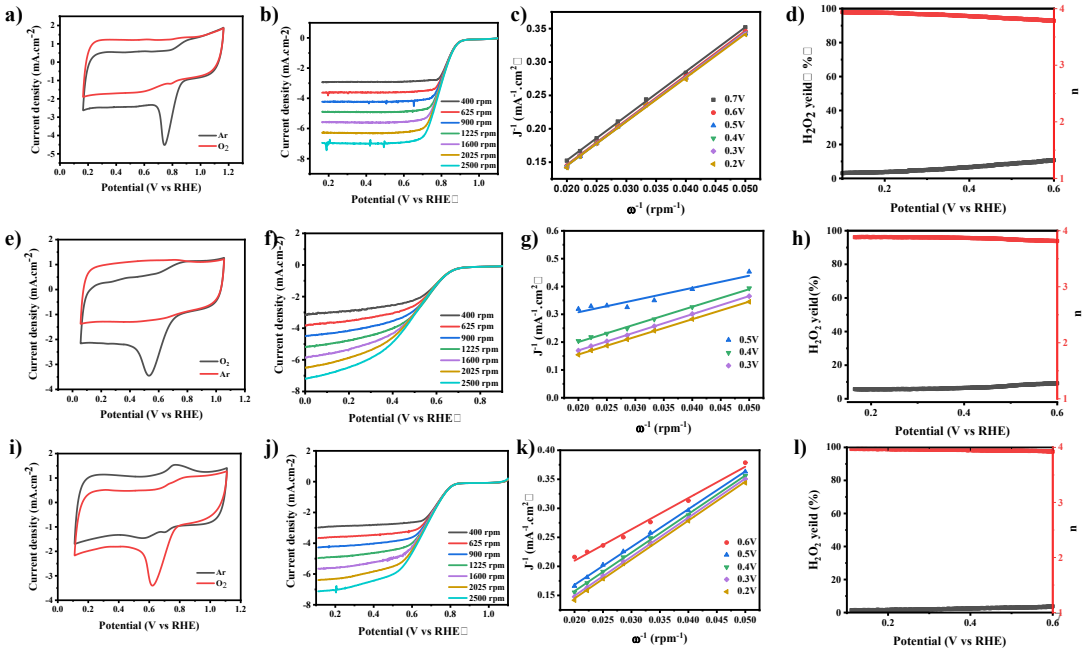

Figure S17. Electrochemical performance of BP-850 in various electrolytes form alkaline conditions to acidic conditions. a) Cyclic voltammograms (CV) of BP-850 obtained in O_2 and Ar saturated in 0.1 M KOH; b) LSV curves of BP-850 at different rotation rates in 0.1 M KOH ; c) K-L plot and the corresponding electron transfer numbers for BP-850 in 0.1 M KOH; d) Percentage of hydrogen peroxide yield and the electron transfer number (n) of BP-850 at different potentials in 0.1 M KOH; e) Cyclic voltammograms (CV) of BP-850 obtained in O_2 and Ar saturated in 0.1 M PBS; f) LSV curves of BP-850 at different rotation rates in 0.1 M PBS; g) K-L plot and the corresponding electron transfer numbers for BP-850 in 0.1 M PBS; h) Percentage of hydrogen peroxide yield and the electron transfer number (n) of BP-850 at different potentials in 0.1 M PBS; i) Cyclic voltammograms (CV) obtained in O_2 and Ar saturated in 0.1 M $HClO_4$; j) LSV curves of BP-850 at different rotation rates in 0.1 M $HClO_4$; k) K-L plot and the corresponding electron transfer numbers for BP-850 in 0.1 M $HClO_4$; l) Percentage of hydrogen peroxide yield and the electron transfer number (n) of BP-850 at different potentials in 0.1 M $HClO_4$ electrolytes.

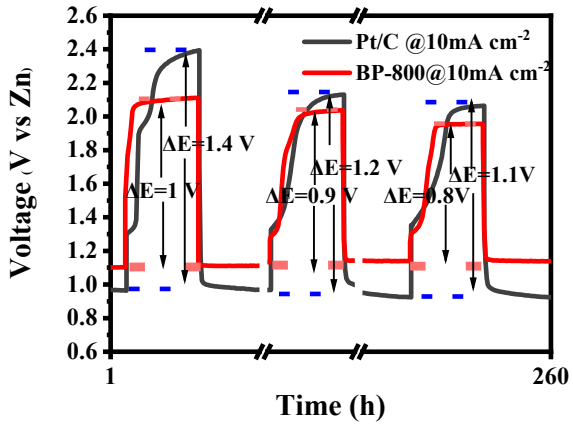

Figure S18. The charge and discharge efficiency at the beginning, middle, and end of the Zn-air battery for the BP-800 and Pt/C-IrO_2 catalyzed battery (the potential gap between the blue line is belonging to the Pt/C-IrO_2 catalyzed battery, and the potential gap between the red line is the battery catalyzed by the BP-800).

Section 7. Supporting Tables

Table S1. Porosity Parameters of prepared polymers and corresponding catalysts.

Sample	S_{BET} (m^2/g)	Pore size (HK) nm	Pore size (BJH) nm	V_{Total} (m^3/g)
BP-CMP	133.3	2.23	2.34	0.13
BP-700	568.9	0.44	1.22	0.386
BP-800	502.7	0.49	1.22	0.408
BP-850-	379.5	0.44	1.22	0.318

Table S2. The surface element contents of different species including carbon, oxygen, nitrogen,cobalt and iron in as-synthesized catalysts, calculated from the XPS spectra

Sample	C (at%)	O (at%)	Fe (at%)	N (at%)	Co (at%)	B (at%)
BP-700	80.5	8.2	1.2	6.3	1.0	2.5
BP-800	85.6	6.2	1.1	4.6	0.7	1.6
BP-850	85.9	5.9	0.9	4.1	0.5	2.4

Table S3. The surface contents of different N species in BP-CMP catalysts, calculated from the XPS spectra

Sample	Pyridinc-N in total N (%)	Fe/Co-N in total N (%)	Pyrrolic-N in total N (%)	Graphitic-N in total N (%)	Oxidized N in total N(%)
BP-700	13.4	8.7	22.6	23.8	31.3
BP-800	16.7	23.4	5.8	38.5	15.3
BP-850	15.3	13.5	14.2	32.6	24.4

Table S4. Summary of various electrocatalysts for ORR in 0.1 M KOH.

Catalyst	E_{Onset} (V)	$E_{1/2}$ (V)	n	Reference
BP-800	**0.93**	**0.80**	**3.79**	**This work**
Single-holed Co/NC hollow particles	0.98	0.87	3.99	S1
Fe-CZIF-800-10	0.98	0.83	3.87	S2
Co/CoNx/N-CNT/C	0.90	0.80	3.77	S3
C_3N_4@NH_2-MIL-101-700	0.99	0.84	3.70	S4
Fe_3C@N-CNT assemblies	0.97	0.85	3.96	S5
(Fe, Co)@NGC	0.91	0.85	3.7	S6
CoFeNx/C	1.01	0.87	3.5	S7
PCN-FeCo/C	1.00	0.85	4.2	S8
FeCo-ISAs/CN	1.00	0.92	4.0	*S9*

Table S5. Summary of various electrocatalysts for ORR in 0.1 M PBS.

Catalyst	Eonset (V)	$E_{1/2}$ (V)	n	Reference
BP-800	**0.85**	**0.66**	**3.79**	**This work**
C_3N_4@NH_2-MIL-101-700	0.92	0.67	3.97	S4
Fe-N/C-800	0.72	0.55	3.97	S10
Fe-P-C	0.84	0.52	3.8	S11
FeIM/ZIF-8	0.91	0.75	3.7	S12

Table S6 Summary of various electrocatalysts for ORR in 0.1 M $HClO_4$.

Catalyst	Eonset (V)	$E_{1/2}$ (V)	n	Reference
BP-800	**0.82**	**0.69**	**3.79**	**This work**
C_3N_4@NH_2-MIL-101-700	0.9	0.65	3.95	S4
Cu-CTF/CP	0.81	0.59	3.7	S13
NPC-1000	1.03	0.818	/	S14
Co-N-C	/	0.731	/	S15

Table S7. The performance of electrically Zn-air batteries with various electrocatalysts.

Catalyst	Loading amount (mg/cm^{-2})	Electrolyte	Peak power density ($mW\ cm^{-2}$)	Open-circuit voltage	Stability
BP-800 (This work)	**1**	**6.0M KOH &0.20M Zn(Ac)**	**184.9**	**1.526**	**75600 min Voltage-gap increased~0.2**
NPMC-1000[S16]	0.5	6.0M KOH	55	1.48	1800 min voltage gap increased~0.7
$Co(OH)_2$+N[S17]	1	6.0M KOH	36	-	3000 min voltage gap increased ~0.2
nanowires/stainless stee[S18]	1.5	6.0M KOH	40	0.98	1000 min voltage Gap increased~0.1
Fe/N-C[S19]	2.2	6.0M KOH &0.20M $Zn(Ac)_2$	40	1.4	1000 min voltage gap increased ~0.16
Fe-N-HPC[S20]	-	6.0M KOH	164.8	1.44	1800 min voltage gap increased ~0.16
$FeNi_3$@NC[S21]	1.0	6.0M KOH &0.20M $Zn(Ac)_2$	139	1.37	1800 min voltage gap increased ~0.16
Fe-N-C[S22]	0.5	6.0M KOH &0.20M $Zn(Ac)_2$	156	1.45	1000 min voltage gap increased ~0.14

Fe-enriched-$FeNi_3/NC$[S23]	1.0	6.0M KOH &0.20M $Zn(Ac)_2$	89	1.43	916 min voltage gap increased ~0.25
FeS_2-CoS_2 /NCFs[S24]	0.5	6.0M KOH &0.20M $Zn(Ac)_2$	69	1.39	1800 min voltage gap increased ~0.3

Section 8. Supporting Reference

1 B. Y. Guan, L. Yu and X. W. (David) Lou, *Adv. Sci.*, 2017, **4**, 1700247.

2 G. Li, J. Zhang, W. Li, K. Fan and C. Xu, *Nanoscale*, 2018, **10**, 9252–9260.

3 H. Zhong, Y. Luo, S. He, P. Tang, D. Li, N. Alonso-Vante and Y. Feng, *ACS Appl. Mater. Interfaces*, 2017, **9**, 2541–2549.

4 W. Gu, L. Hu, J. Li and E. Wang, *ACS Appl. Mater. Interfaces*, 2016, **8**, 35281–35288.

5 B. Y. Guan, L. Yu and X. W. (David) Lou, *Energy Environ. Sci.*, 2016, **9**, 3092–3096.

6 J. Xi, Y. Xia, Y. Xu, J. Xiao and S. Wang, *Chem. Commun.*, 2015, **51**, 10479–10482.

7 R. Jiang and D. Chu, *J. Power Sources*, 2014, **245**, 352–361.

8 Q. Lin, X. Bu, A. Kong, C. Mao, F. Bu and P. Feng, *Adv. Mater.*, 2015, **27**, 3431–3436.

9 D. Zhang, W. Chen, Z. Li, Y. Chen, L. Zheng, Y. Gong, Q. Li, R. Shen, Y. Han, W.C. Cheong, L. Gu and Y. Li, *Chem. Commun.*, 2018, **54**, 4274–4277.

10 L. Lin, Q. Zhu and A.-W. Xu, *J. Am. Chem. Soc.*, 2014, **136**, 11027–11033.

11 K. P. Singh, E. J. Bae and J.S. Yu, *J. Am. Chem. Soc.*, 2015, **137**, 3165–3168.

12 D. Zhao, J.L. Shui, C. Chen, X. Chen, B. M. Reprogle, D. Wang and D.-J. Liu, *Chem. Sci.*, 2012, **3**, 3200–3205.

13 K. Iwase, T. Yoshioka, S. Nakanishi, K. Hashimoto and K. Kamiya, *Angew. Chemie Int.*

Ed., 2015, **54**, 11068–11072.

14 L. Ye, G. Chai and Z. Wen, *Adv. Funct. Mater.*, 2017, **27**, 1606190.

15 B. You, N. Jiang, M. Sheng, W. S. Drisdell, J. Yano and Y. Sun, *ACS Catal.*, 2015, **5**, 7068–7076.

16 J. Zhang, Z. Zhao, Z. Xia and L. Dai, *Nat. Nanotechnol.* 2015, **10**, 444–452.

17 B. Li, X. Ge, F. W. T. Goh, T. S. A. Hor, D. Geng, G. Du, Z. Liu, J. Zhang, X. Liu and Y. Zong, *Nanoscale*, 2015, **7**, 1830–1838.

18 D. U. Lee, J.Y. Choi, K. Feng, H. W. Park and Z. Chen, *Adv. Energy Mater.*, 2014, **4**, 1301389.

19 J. Wang, H. Wu, D. Gao, S. Miao, G. Wang and X. Bao, *Nano Energy*, 2015, **13**, 387–396.

20 D. Wang, H. Xu, P. Yang, L. Xiao, L. Du, X. Lu, R. Li, J. Zhang, M. An, *J. Mater. Chem.A,* 2021, **9**, 9761-9770.

21 D. Chen, J. Zhu, X. Mu, R. Cheng, W. Li, S. Liu, Z. Pu, C. Lin, S. Mu, *Appl. Catal. B*, 2020, 268,118729.

22 R. Yuan, W. Bi, T. Zhou, N. Zhang, C.a. Zhong, W. Chu, W. Yan, Q. Xu, C. Wu, Y. Xie, *ACS Mater. Lett.*, 2019, **2**, 35-41.

23 K. Chen, S. Kim, R. Rajendiran, K. Prabakar, G. Li, Z. Shi, C. Jeong, J. Kang, O.L. Li, *J Colloid Interface Sci*, 2021, **582**, 977-990.

24 X. Shi, B. He, L. Zhao, Y. Gong, R. Wang, H. Wang, *J. Power Sources*, 2021, **482**, 228955.